

# Ignition improvement by injector arrangement in a multi-fuel combustor for micro gas turbine

O. Antoshkiv<sup>1,\*</sup>, T. Poojitganont<sup>1</sup>, S. Jeansirisomboon<sup>2</sup> and H. P. Berg<sup>1</sup>

<sup>1</sup> BTU Cottbus - Senftenberg, Siemens-Halske-Ring 14, Cottbus, 03046, Germany

<sup>2</sup> Gulf Group Company, 67 Wireless Road, Bangkok, 10330, Thailand

\* Corresponding Author: antoshki@b-tu.de

**Abstract.** The novel combustor design also has an impact on the ignitor arrangement. The conventional ignitor system cannot guarantee optimal ignition performance in the usual radial position. The difficult ignitability of gaseous fuels was the main challenge for the ignitor system improvement. One way to improve the ignition performance significantly is a torch ignitor system in which the gaseous fuel is directly mixed with a large amount of the combustor air. To reach this goal, the ignition process was investigated in detail. The micro gas turbine (MGT) ignition was optimised considering three main procedures: torch ignitor operation, burner ignition and flame propagation between the neighbour injectors. A successful final result of the chain of ignition procedures depends on multiple aspects of the combustor design. Performed development work shows an important step towards designing modern high-efficiency low-emission combustors.

## 1. Introduction

The decentralization of electric energy generation requires development of modern powerful and environmental friendly co-generators. The micro gas turbine (MGT) is a power system with low maintenance costs. Furthermore, a gas turbine can operate by using different fuels. The limited fossil energy sources and increasingly stringent emission regulations demand today an environmental friendly combustion technology, working on alternative fuels. This leads to a new combustion chamber architecture. In comparison to the conventional combustor, the multi-fuel combustion chamber operates under a higher swirl number and longer dilution zone. Due to this fact, the combustor prepares much homogeneous air-fuel mixture, which causes lower NO<sub>x</sub>-emissions.

Combustion is the basic of technology concerning operation of internal combustion engines. However, it is considered to be the main source of pollution in the natural environment that can threaten inhabitants. Since the pre-industrialized era, Green House Gas (GHS) concentration is continuously observed, and it is found that in 2012 CO<sub>2</sub> was about 40% higher than in the mid-1800s. Among human activities that produce greenhouse gases, the use of energy is by far the largest source of emission (around 83%). Within energy sector, oxidation of CO<sub>2</sub> during combustion dominates the total GHG emissions [1].

A gas turbine is an energy converter that change chemical energy contained in fuel to mechanical energy. In the energy sector, gas turbine usually cooperates with generator in an effort to convert mechanical energy to electrical energy. Main components of general gas turbine are compressor, combustor, and turbine. First of all, air is compressed into high pressure condition by multi stages of compressor, following that air and fuel well mix in a combustion zone and initially ignited by spark



igniters. Gas turbine burner can be considered as a decisive part of combustor placed in a combustion chamber, where compressed air and fuel are mixed. It can be classified as premixed or non-premixed burner types. An ideal burner should guarantee complete combustion, flame stability, low emissions and high reliability in a wide range of operation condition [2], even if in an unexpected situation. Figure 1 (left) illustrates burner configurations for specific types of fuels, which is designed by BTU Cottbus-Senftenberg's researchers for a micro gas turbine (MGT) [3].

## 2. Previous research work

One crucial demanded characteristics of gas turbine combustor is ability for fast and reliable flame transfer from operated burner to others. This flame transport can be described a light-across phenomenon, which is a part of a light-around phase that flame is distributed to all burners in a combustion chamber. In principle, flame propagation is influenced not only by a volumetric expansion, but also buoyancy force and burner aerodynamics [4-5]. Almost of practical combustors consist typically of multi-burners placed side-by-side around its periphery similar to combustor demonstrated in figure 1 (right).

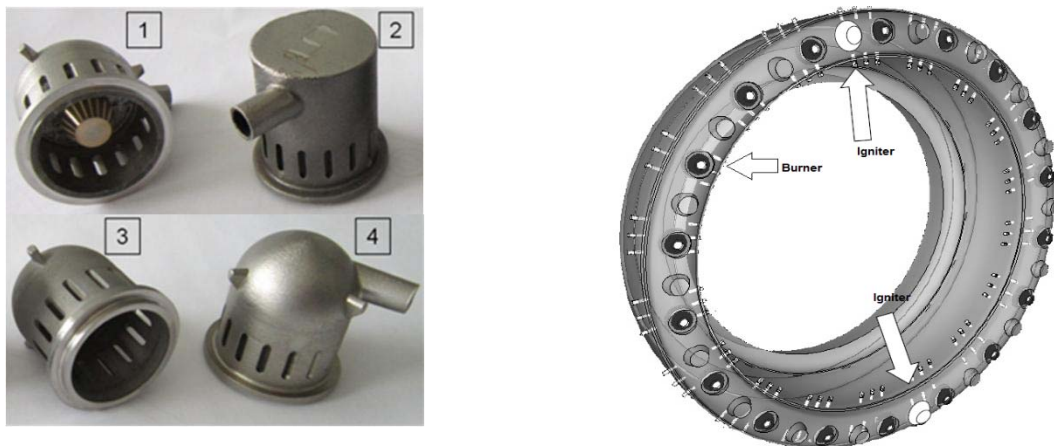


**Figure 1.** MGT Kerosene/Diesel Injector (1), Methane/Natural Gas Burner (2), LNG Injector (3), INSBruk™ Burner (4) and Turbomeca Vesta combustor 18 main burners and 2 igniters [4,6-7].

The non-reacting direct numerical simulation of twin swirling jet at  $Re = 5000$  with 3 swirl levels ( $S = 0.68, 1.08$  and  $1.42$ ) was investigated in order to study the interaction between swirling jet burners. This study showed that twin swirl jets strengthen and augment turbulence and Reynolds stress, compared with an isolated one because of the aerodynamic interaction of consecutive burners. In addition, the higher swirl number leads to the larger intensive interaction between burners as shown in figure 2 [8]. In consistent, Kao Y.H. et al. [9] proposed that multi-burner aerodynamic profile is different from a single burner as it is also concerned with adjacent burner interaction even if for a cold-flow (non-reacting). Moreover, not only the inter-swirler space influenced on multi-burner aerodynamics and flow field profiles, but it is also affected by the distance of burners to the walls [9].

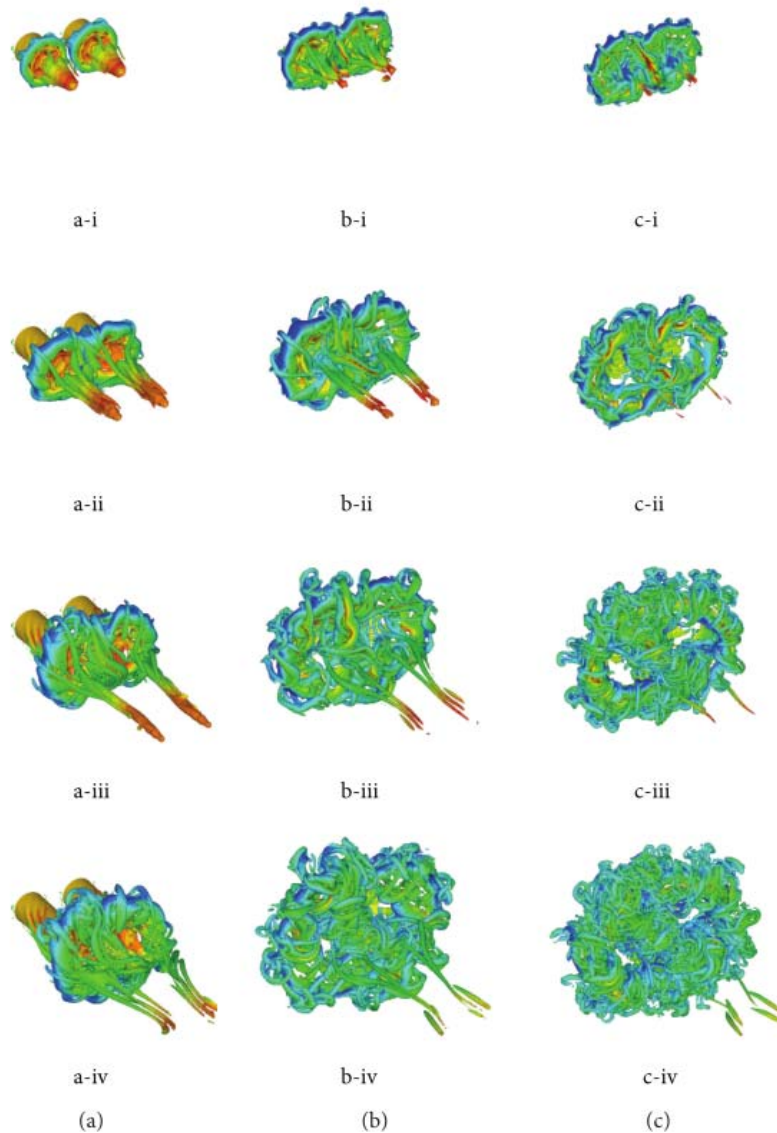


**Figure 2.** The twin swirling jet burner interaction with different swirl number  $s=0.68$  (a),  $s=1.08$  (b) and  $s=1.42$  (c) from  $t=2.5$  ms to 10 ms (from I to IV correspondingly) [8].

A large eddy simulation of a complete gas turbine chamber was conducted in 2013. It is important that thermal expansion played a great role on the flame propagation to neighbour burners rather than turbulence because the flame front moved at faster speed than turbulent flame speed [6, 10].

Not only, interconnection of consecutive burner aerodynamics and thermal expansion influence on flame propagation, but distance also affects flame dynamics. Barré, D. et al. studied methane/air non-premixed combustion and addressed that the ignition sequence strongly depends on the spacing of burners. If spacing increases, axial propagation becomes dominant and successive time to a full ignition also rises in figure 3 [7].

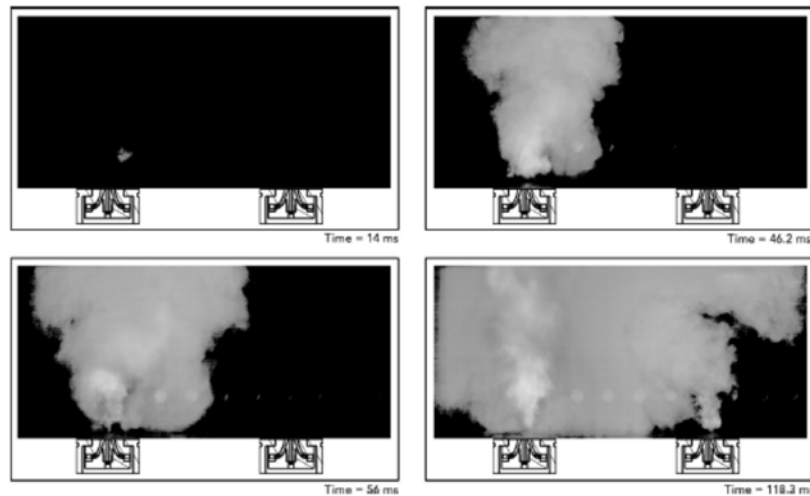


**Figure 3.** Fast visualization of flame dynamics for large distance between burners [7].

It is obvious that increasing space between burners leads to a lower flame propagation possibility. In consequence, burner angle was implemented in order to improve light-across ignitability performance and ease the difficulty of large distance light-across. Figure 4 demonstrates the typical burner arrangement in the MGT combustor developed at the BTU Cottbus - Senftenberg.

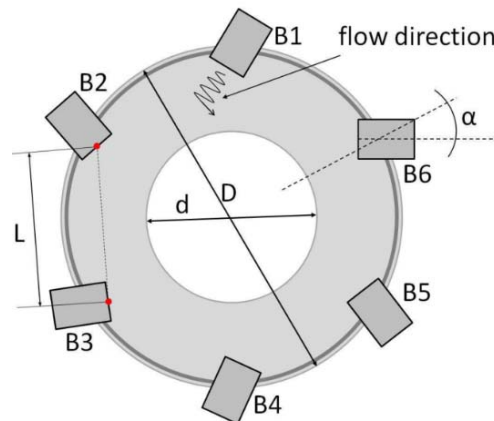


**Figure 4:** MGT Burners arrangement [11].

### 3. Experimental Configuration

#### 3.1. Test hardware

Experimental burner has a configuration showed in figure 5 and mounted around the periphery of MGT combustion chamber in operation (figure 6). In the case of this experiment, a combustion liner is designed in order to place burner inside. Gas is supplied circumferentially through 8 millimetres diameter inlet at the bottom of the cup and distributed through 15 small holes (figure 5).

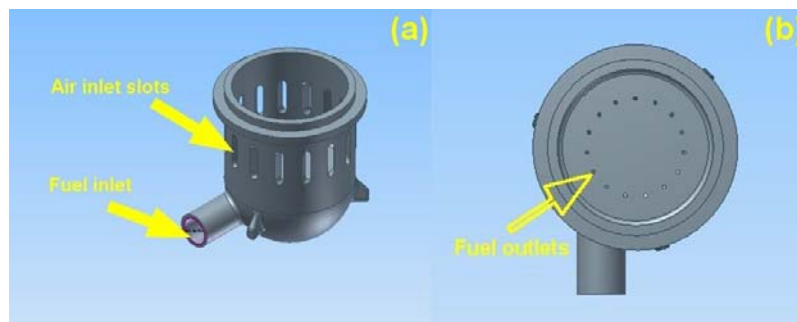


**Figure 5.** Burner configuration isometric view (a) and top view (b).

Whereas surrounding air inside the combustor frame flows through 15 swirling vane slots on the symmetric circumference of the burner surface, creating swirling flow in order to stabilize flame.

In this experiment two identically aligned burners are placed on aluminium profiles, which can be linearly adjusted to change the distance between burners, whereas the limit of the nearest and farthest spaces is defined by the diameter of flame tube and the dimensions of combustion liners. In addition, angle orientation is adapted by an adjustable aluminium connector with an angle lock screws.

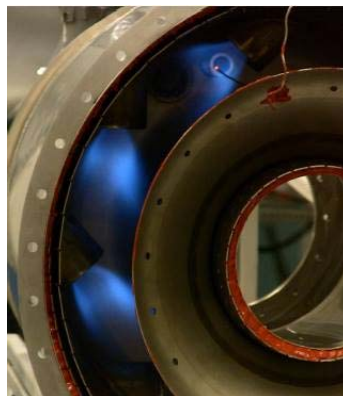


**Figure 6.** Position of burners in real MGT combustor.

Air and fuel are mixing at atmosphere condition. A fixed spark ignitor operates at a voltage range between 5-10 kV near the centre of the burner provides energy to create a spark kernel. In addition, overall fuel mass flow rates are controlled by a Bronkhorst flow meter model F-103D with the operation flow rate 1.5 g/sec and temperature 20 °C at 1 bar. After that, a fuel flow divides to distribute fuel equally to all burners. Similarly, air is supplied by an air compressor unit with a maximum capacity of 60 g/s at operating atmospheric pressure. According to the schematic (figure 7), compressed air flow rate is adjusted by a by-pass control valve and compressed air passes through an air distributor.

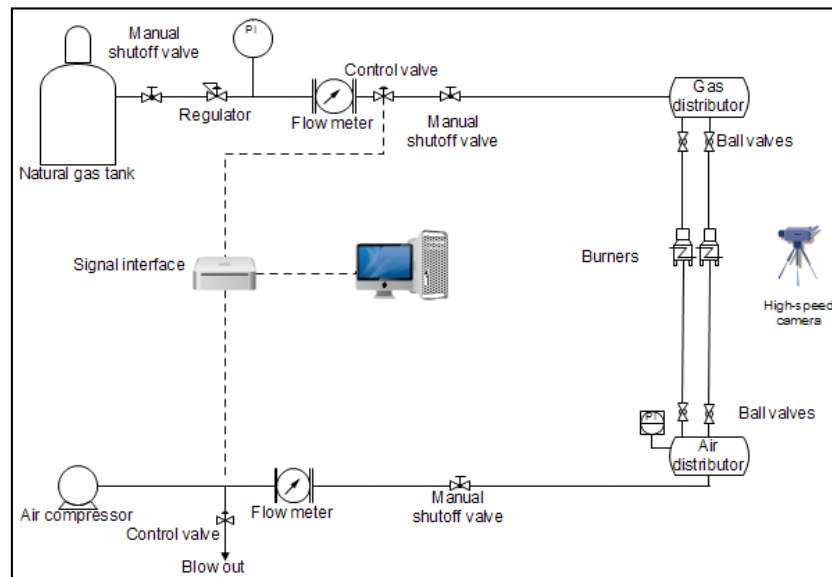


**Figure 7.** Experimental schematic set-up.

In order to observe flame propagation among variation of equivalence ratios, all valves are controlled by in-house software programmed in LabVIEW. Pressure gauges are used to monitor both air and fuel pressure locally without data interface. The uncertainty of the data during experiment could be claimed that it is lower than 5% as usual.

### 3.2. High-speed imaging system

General components arrangement at the test rig is shown in figure 8. The combustor chamber walls consist of quartz glasses with sealing between their edges at aluminium profiles. On the back side, a black screen is placed in order to facilitate observation and picture taking. High-speed camera system consists of IRO connected with phantom high speed camera. IRO and high-speed controllers control the trigger and interface with the Davis software [12].

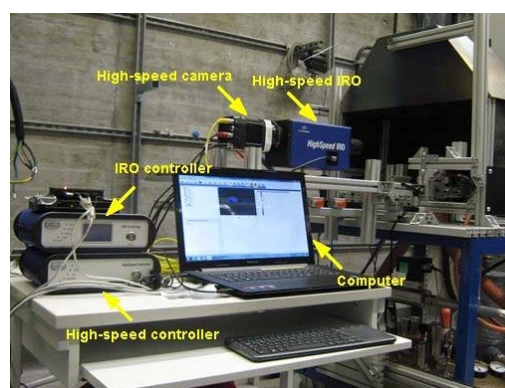


**Figure 8.** High-speed camera system components.

## 4. Discussion of results

All of propane-air mixture combustion experiments were conducted at the atmospheric condition. Temperature and pressure are around 25 °C at humidity 51% and 1004.11 mbar with a constant air mass flow rate at 6 g/s. The mass flow rate shown in the pictures is averaged over the numbers of experiments ( $\dot{m}_{avg}$ ). The experimental conditions are shown in table 1 with the increased step of distance until



reaching 70 mm with at least 3 experiments at each condition. Flame colour is blue. Flame enlargements in both axial and horizontal directions according to rising amount of fuel mass flow (figure 9).

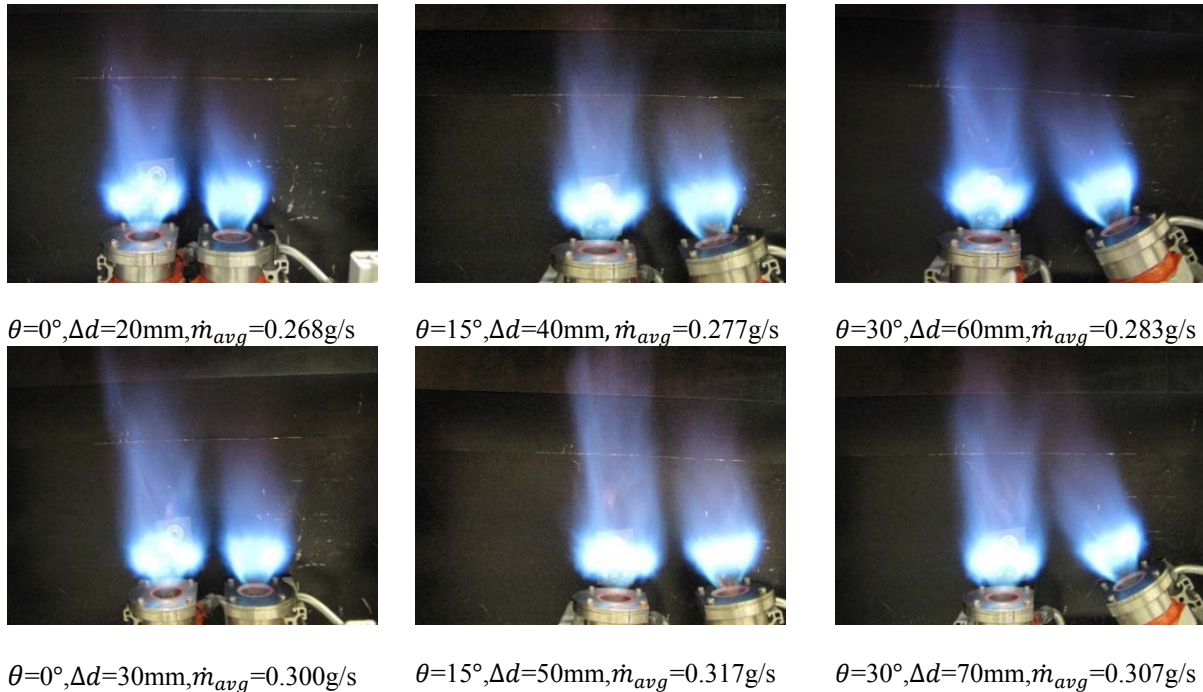


**Figure 9.** Flame feature at different fuel mass flow rates.

Required fuel mass flow rate provoked flame propagation at various burner spaces and tilted angles as illustrated in figure 10. It is obvious that all tilted angles have excellent linear relation of distance and fuel mass flow for all interested ranges with minimal experiment deviation as an error bar. Among all angles, 75° required less fuel mass flow for the flame jump. The larger tilted angle, the smaller amount of fuel is necessary to achieve flame propagation.

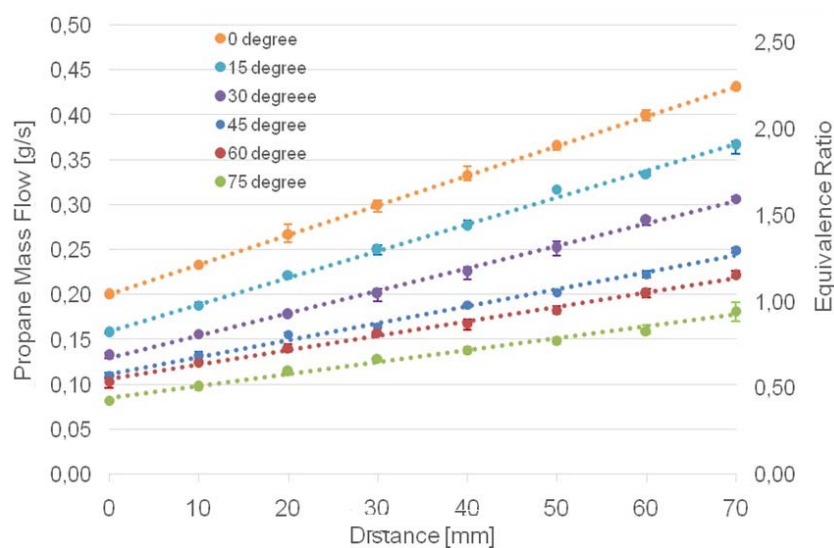


**Figure 10.** Mass flow rate and distance relation of all tilted angles with error bar.

In order to evaluate flame propagation capability between consecutives burners [2], dimensionless term, called ignitability unit ( $I_{ig}$ ), is introduced in order to compare the capability of flame propagation among particular conditions.

$$I_{ig} = \frac{1}{\phi} = \frac{AFR_{LACR}}{AFR_{stoich}} \quad (1)$$

Data in figure 10 are shown to explain the relation of ignitability unit as a function of distance and burner angles which is illustrated in figure 11. Curves were fitted using the least-squares method of polynomial order 2 for the points approximation. The approximated mathematical functions are shown in table 1. Additionally, experiment pictures of all angles (15°, 30°, 45°, 60°, and 75°) are also available in the appendix.

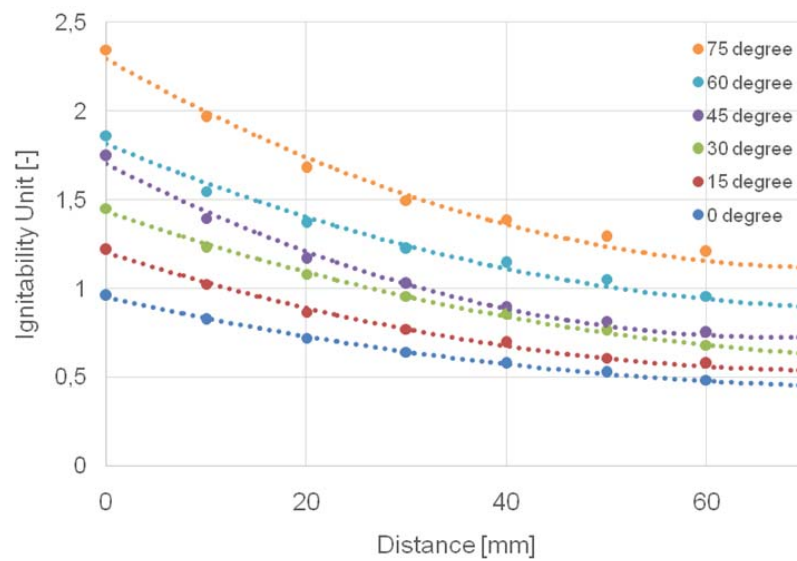


**Figure 11.** Ignitability unit and distance relation at all tilted angles.

It is noticeable that 75° achieves ignitability units above unity for all interested distance. In contrast with 0° position, it was not able to surplus unity for all lengths. While the others have both ignitability higher and lower unity.

**Table 1.** Approximated formulas of ignitability unit by the least-squares method.

Tilted angle	$I_{ig} = f(d); I_{ig} = \text{ignitability}; \Delta d = \text{distance}$
0°	$I_{ig} = 0.00008\Delta d^2 - 0.0126\Delta d + 0.9492$
15°	$I_{ig} = 0.0001\Delta d^2 - 0.018\Delta d + 1.2014$
30°	$I_{ig} = 0.0001\Delta d^2 - 0.0193\Delta d + 1.4322$
45°	$I_{ig} = 0.0002\Delta d^2 - 0.0292\Delta d + 1.704$
60°	$I_{ig} = 0.0001\Delta d^2 - 0.0235\Delta d + 1.8143$
75°	$I_{ig} = 0.0002\Delta d^2 - 0.032\Delta d + 2.2931$

In order to illustrate the relation of all parameters, surface plot was implemented to explain ignitability as a function of tilted angle and distance (figure 12). It is visible that the larger distance of



consecutive burners, the lower ignitability at all tilted degrees is required. Moreover, larger burner angle leads to higher ignitability at specific distance, compared with smaller one. Among all angles, the highest ignitability is clearly at the 75° and descended to 0°.

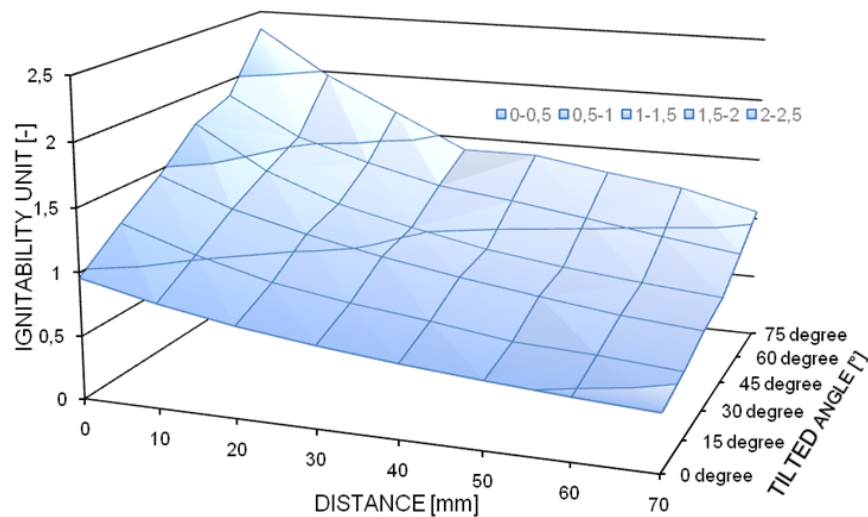


**Figure 12.** Ignitability unit as a function of distance and tilted angle in surface plot.

## 5. Experimental Investigation of Flame Propagation

### 5.1. Conditions of performed experiments

In order to investigate the dynamics of flame propagation is enough to observe the tracking of OH radicals using OH\* light. The high-speed imaging system was used for this aim. To avoid the heat effect on high-speed system and for safety operating condition for high-speed imaging investigation, the fuel mass flow was adjusted at 0.3 g/s ( $\phi < 1$ ). Tilted angle 0° degree, which is norm of gas turbines, and 45 degree, which is intermediate angle, are of interest. The experimental conditions and settings of the high-speed camera were identical during all performed tests.

During the experiments, air mass flow rate has been fixed at 6 g/s, whilst burners distance and tilted angles are varied in the range of 0-70 mm and 0°-75°, respectively. Fuel mass flow rates of each specific cases providing successive flame propagation were defined. It is understandable that larger distances required higher fuel flow rates to maintain flame jump to another burner. At distance 70 mm of tilted angle 0°, the largest overall fuel mass flow of 0.864 g/s was needed.

### 5.2. Example of Tilted Angle 0° and Distance 15 mm

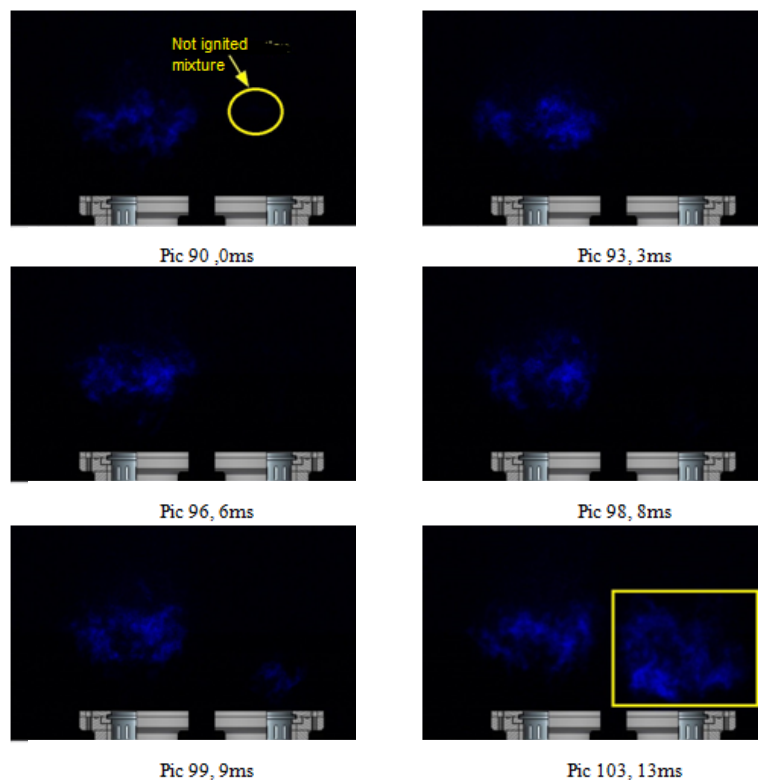
The important experimental conditions and the high-speed camera parameters are illustrated in table 2.

**Table 2.** Experimental conditions of tilted angle  $0^\circ$  with distance 15 mm.

Experimental Parameters	Values
$\dot{m}_{air}, [g/s]$	0.6
$\dot{m}_{C_3H_8}, [g/s]$	0.5
$T, [^\circ C]$	27
$P, [atm]$	1
$RH\%, [\%]$	44
$Gain, [-]$	40
$Gate, [ns]$	200 000
$Exposure\ Time, [\mu s]$	229.805

Figure 13 shows the recorded distribution of  $OH^*$  during light-across. Until the reactive particles reach second burner, it moves toward downstream of the second burner in an axial direction into the recirculation zone. After it arrives the region near the outlet of the consecutive burner, higher light emission was observed and the concentration of  $OH^*$  increased significantly, following shortly by a fully develop of the combustion reaction (Pic.103). Finally, the steady state of reaction was achieved with lower  $OH^*$  distribution and with the smaller region of  $OH^*$  territory, compared to the previous stage; however, it showed quite steady location without considerable movement.

Large amount of gray scale high-speed pictures are exported by DaVis and post-processing to measure light intensity by the software called ImageJ, where the quantity of light intensity is normalized by its maximum value over the observed time period was conducted in order to present a better comparison of the light intensity degree at particular times.

**Figure 13.** Snap-shots of  $OH^*$  dynamics at tilted angle  $0^\circ$  and distance 15 mm with 1K resolution.

Normalized-light intensity (figure 14) over time was observed and is demonstrated in the box in Pic. 103 of figure 13. The figure shows OH\* distribution during obvious stages of development of flame propagation. In the first step, light intensity (OH\*) of second burner is not indicated. A formed cloud starts travelling to downstream (Pic. 90-98). In other words, higher ignition energy is generated, which is enough to ignite second burner. Finally, complete ignition of the consecutive burner is noticeable with the medium light intensity fluctuation.

The plot in figure 14 shows the time development of normalized-light intensity at 0° tilted angle and distance 15mm achieved after data acquisition.

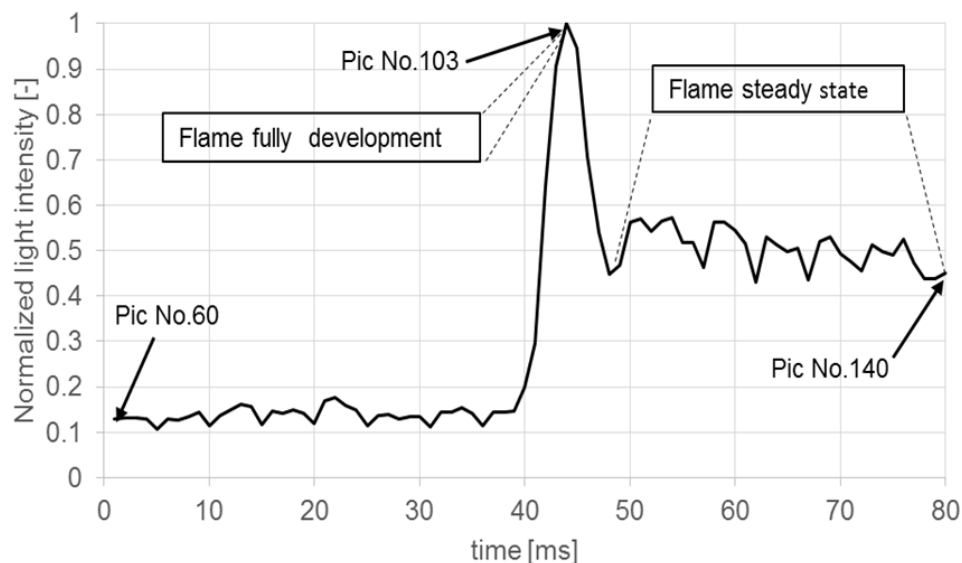


**Figure 14.** Time development of normalized-light intensity at 0° tilted angle and distance 15mm.

## 6. Conclusions

Test rig with twin burners has been implemented to study the correlation of the distance between burners and their tilted angles in order to get a better understanding of the condition driving a light-across ignition phenomenon. The methodology applied for the experiments were also contributed rationally in detail.

The relationships between equivalence ratios of ignition and distances of all tilted angles show apparently linear trends (figure 10). The Ignitability unit, which is a reciprocal of global equivalence ratio, was introduced as a parameter to evaluate and compare flame propagation potential among experimental cases. Tilted angle 75° degree performed the highest ignitability above unity at all interested distance, compared with the others (figure 12). In other words, the greater tilted angle, the larger distance between burners can be achieved at a particular ignitability unit. It was found that a tilted burner angle compensates a difficulty of a larger distance between burners and facilitates leaner combustion.

Flame behaviour at 15 mm of tilted angle 0° and 60 mm of 45° were examined by LaVision's high-speed imaging system equipped with OH\* filter in order to eliminate interfered wave lengths. OH\* radical behaviour of both cases were almost the same. OH\* appeared rarely in the region of an unignited burner at a lower equivalence ratio. Increasing the equivalence ratio, OH\* accumulated and augmented to be a cloud at the downstream region. At this state, the cloud moved upstream to an unignited burner (figure 13). Until it reached a lower area near the outlet of burner, OH\* quantity enlarged substantially over a territory and the highest light intensity emitted at this state. Finally, OH\* concentration decreased with shrinking in dispersed areas to a steady condition with lower light emissions and a minor fluctuation beyond this timeframe.

The results provide a hint and highlight an approach to increase gas turbine ignitability and mitigate a flame propagation trouble of consecutive burners for lean and ultra-lean combustions. Possibility to reduce burner units around combustion chamber is accessible as a result in lower weight per unit of power output, cost effectiveness and less maintenance expenses. In addition, the data can be used for validating computational simulations of combustion flame propagation as a benchmark and offering more insights of the light-across phenomenon.

Other aspects of properties such as local equivalence ratios, local temperature, element chemical compositions, etc. are also beneficial for better understanding the nature of excited radicals, promoting flame propagation across sectors as well.

## References

- [1] International Energy Agency 2013 *CO<sub>2</sub> Emission from Fuel Combustion Highlights* (Paris: IEA)
- [2] Lefebvre A H and Ballal D R 2010 *Gas Turbine Combustion* (Philadelphia: Taylor & Francis)
- [3] Antoshkiv O, Berg H P and Mundstock J 2013 *Conf. 26. Deutscher Flammentag* Duisburg-Essen
- [4] Boileau M, Staffelbach G, Cuenot B, Poinot T and Bérat C 2008 *Combustion and Flame* **154** 2
- [5] Bach E, Kariuki J J, Dawson R and Mastorakos E 2013 *Conf. 51st AIAA Aero. Sci. Meeting* Grapevine (Dallas/Ft. Worth Region)
- [6] Bourgouin J F, Durox D, Schuller T, Beaunier J and Candel S 2013 *Combustion and Flame* **160** p 1398
- [7] Barré D, Esclapez L, Cordier M, Riber E, Cuenot B, Staffelbach G, Renou B, Vandel A, Gicquel L Y and Cabot G 2014 *Combustion and Flame* **161** p 2387
- [8] Xu W, Gui N, Ge L and Yan J 2014 *J. of Computational Engineering* **2014**
- [9] Kao Y, Tambe SB, Jeng S 2014 *Proc. ASME. Turbo Expo vol 4A* (Düsseldorf)
- [10] Warnatz J, Maas U and Dibble R W 1996 *Combustion* (Hiedelberge: Springer)
- [11] Antoshkiv O, Berg H P, Jobusch C and Poojitganont T 2013 *Proc. XXI Int. Sym. on Air Breathing Engines vol 2* p 1217
- [12] LaVision GmbH 2014 *DaVis 8.2 software* (Göttingen: LaVision GmbH)